Journal of Catalysis **198,** 41–46 (2001)
doi:10.1006/jcat.2000.3128, available online at http://www.idealibrary.com on IDEAL®

Examination of Coked Surfaces of Pillared Rectorite Catalysts with the Atomic Force Microscope

M. L. Occelli*,[1] and S. A. C. Gould†

*MLO Consulting, 6105 Black Water Trail, Atlanta,Georgia 30328; and †W. M. Keck Science Center, Claremont Colleges, Claremont, California 91711

Received June 1, 2000; revised November 21, 2000; accepted December 4, 2000; published online February 1, 2001

The reaction of a sample of natural rectorite with an aluminum chlorhydroxide solution containing the dodecameric $[Al_{13}O_4(OH)_{24}(H_2O)_{12}]^{7+}$ ion generates a heat-stable microporous structure with surface area available to sorption and catalysis. An atomic force microscope (AFM) operating in contact mode has produced images showing that the pillared rectorite surface is free from Al species, implying that all the $[Al_{13}O_4(OH)_{24}(H_2O)_{12}]^{7+}$ ions are located inside the clay montmorillonite-like layers. As expected, nanometer-scale images of the clay tetrahedral sheet show a surface that consists of rings of basal oxygens arranged in a hexagonal symmetry. White spots, representative of the three basal oxygens of SiO_4 tetrahedra, have repeat distances of 0.54 and 0.97 nm, respectively, in close agreement with the rectorite unit cell dimensions. Thermal and hydrothermal treatments used to prepare the pillared rectorite for microactivity testing (MAT) have little effect on the molecular parameters of the clay surface. After cracking gas oil under MAT conditions, AFM images of the spent clay catalyst reveal that surface carbon preferentially deposited on or near the three basal oxygens of the SiO_4 units that constitute the clay silicate layer. As a result, nanometer-scale images of the coked pillared clay surface contain well-defined hexagonal arrangements of white spots having next-neighbor and lateral distances of 0.70 and 1.23 nm that exclude the possibility of graphite formation. After regeneration in flowing air at 760°C/2 h to remove carbon deposits, the pillared clay catalyst resumes its original coloration and the nanometer-scale parameters of the rectorite surface are restored.

INTRODUCTION

Rectorite is an interstratified layered silicate mineral consisting of a regular (1 : 1) stacking of mica-like layers and montmorillonite-like layers (1). Thus only the montmorillonite-like layers can exchange charge-compensating mono- and divalent cations with large polyoxocations of Al (or Zr) to form a microspace separated by two silicate layers that impart to the pillared rectorite its zeolite-type thermal and hydrothermal stability. A schematic representation of the rectorite structure is given in Fig. 1A. Pillared rectorite catalysts are clays expanded with $[Al_{13}O_4(OH)_{24}(H_2O)_{12}]^{7+}$ ions that, on heating, form microporous materials with thermal and hydrothermal stability similar to that of zeolites with the faujasite structure used in fluid cracking catalyst (FCC) preparation (2–4). After steaming for 5 h under microactivity test (MAT) conditions (100% steam at 760°C and 1 atm), pillared rectorites can crack gas oil with 85.2% conversion and 59.5% gasoline generation (4). However, coke generation (10.2%) remains high. In fact, coke formation on pillared clay was found to be at least twice as large as in HY-type zeolites (5). The Lewis acidity of the clay catalyst is believed to promote polycondensation reactions and high coke formation.

Coke formation on catalysts has traditionally been investigated by infrared and X-ray photoelectron spectroscopies. Imaging of coked surfaces has been accomplished using scanning tunneling microscopy (6) and high-resolution electron microscopy (7). Micrometer-scale (5×5 μm) atomic force microscopy images have shown that on a partial oxidation catalyst such as MoO_3, coke deposition forms 10-nm particles organized in rows parallel to the [010] direction of the crystal (8).

It is the purpose of this paper to describe the use of an atomic force microscope (AFM) operating in contact mode to study changes that the surface of a pillared rectorite catalyst undergoes after thermal and hydrothermal treatments and gas oil cracking. Nanometer-scale features of the surface after coke deposition and regeneration are also described in detail. The utility of the AFM to study the surface topography and the molecular structure of clay mineral surfaces has already been demonstrated by several authors (9–12).

EXPERIMENTAL

The natural rectorite sample from Garland County, Arkansas, and the preparation of a pillared catalyst with aluminum chlorhydroxide (ACH) solutions have been described in another paper (4). The pillared rectorite under study has surface area of 155 m^2/g and pore volume of

[1] To whom correspondence should be addressed.

0021-9517/01 $35.00

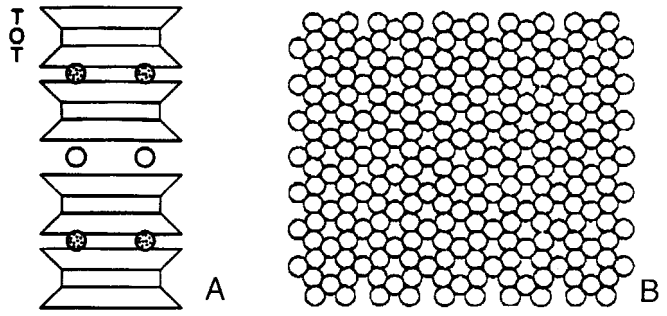

FIG. 1. (A) Schematic representation of the rectorite structure. The T–O–T three-layer sequence (T = tetrahedral, O = octahedral sheet) is represented by trapezoids and rectangles. Exchangeable and nonexchangeable charge-compensating cations are represented by open and solid circles. (B) The (001) view of the rectorite tetrahedral sheet.

0.10–0.12 cm^3/g. Calcination of the pillared rectorite catalyst was accomplished by heating in air at 540°C/10 h. Steam aging was then performed by passing steam at 760°C over the catalyst for 5 h. MAT of these materials has been described in detail elsewhere (4).

The AFM used for these experiments was a microscope (Nanoscope II head with Nanoscope III data acquisition system) from Digital Instruments operating in contact mode and calibrated by imaging mica. Rectorite and pillared rectorite flakes were glued onto stainless-steel disks with epoxy resin. After the glue dried, the AFM tip was carefully placed in the middle of a flake; mica was used as an internal standard. The images reported contain 256×256 data points and nearly all images were acquired at a scan rate of 10–20 lines/s. The Si_3N_4 cantilevers (with integral tips) used for imaging were 120 μm in length and possessed a spring constant of 0.6 N/m. The force applied was about 1 nN; this information was obtained using the force calibration technique contained in the AFM software package. A total of 125 images were obtained in the present study.

The procedure for selecting images and for reporting the means and standard deviations for the data in Table 1 was as follows. A two-dimensional fast Fourier transform (2DFFT) of the image was first calculated using the standard Nanoscope III software. Locations of major peaks were then measured. In an image where the highlight is rows of white spots as in Figures 2 and 3, the 2DFFT is a hexagon

TABLE 1

Molecular Parameters (in nm) of the Pillared Rectorite Surface after Thermal Pretreatments, Gas Oil Cracking under MAT Conditions, and Regeneration in Air at 760°C/2 h[a]

ACH-rectorite	d_c	SD	d_l	SD	No. of images
Calcined	0.54 ± 0.02	0.013	0.97 ± 0.04	0.029	18
Steamed	$0.52 + 0.05$	0.014	0.90 ± 0.05	0.030	6
Coked	0.70 ± 0.05	0.020	1.23 ± 0.05	0.020	13
Regenerated	$0.54 + 0.05$	0.020	$0.94 + 0.05$	0.040	4

[a] Next-neighbor and lateral distances between white spots are given by d_c and d_l. The parent natural rectorite has d_c and d_l values of 0.54 and 0.96 nm, respectively.

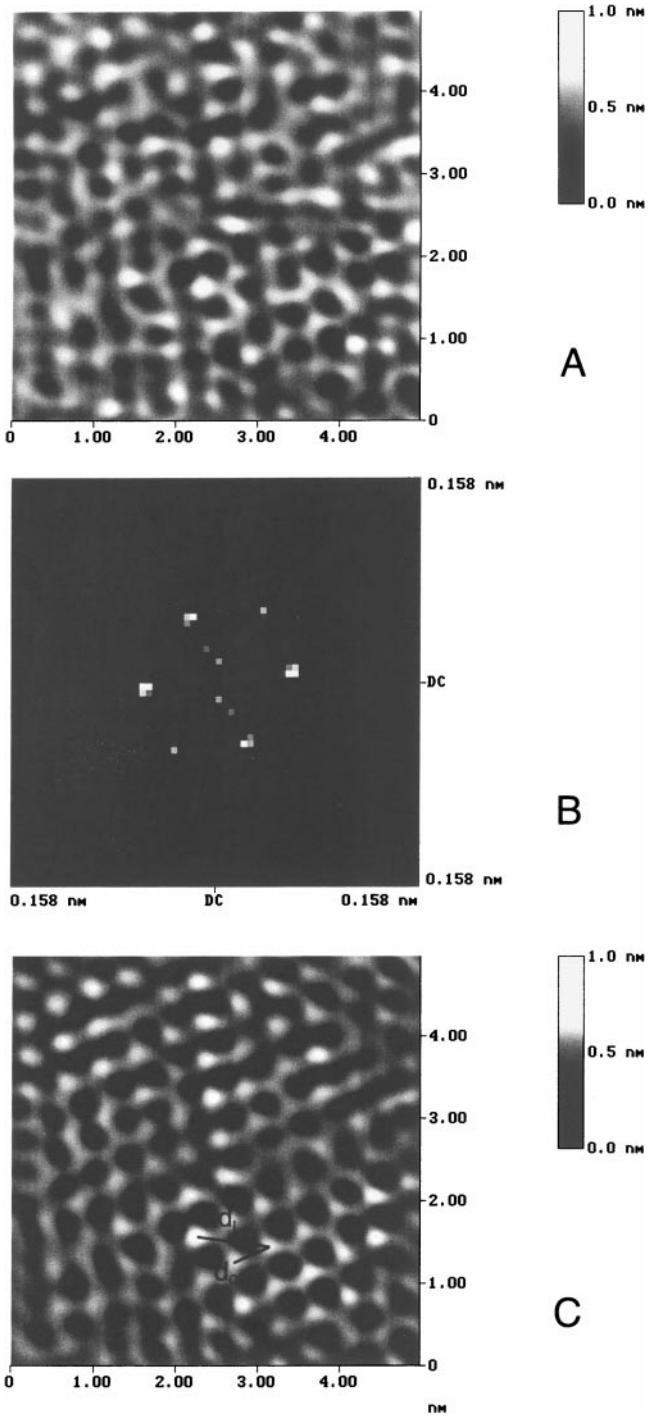

FIG. 2. Contact mode AFM images of the (001) plane of the calcined pillared rectorite: (A) raw image; (B) 2DFFT spectrum; (C) filtered image after application of a 2DFFT routine with the FFT attenuation band cutoff set to 8.

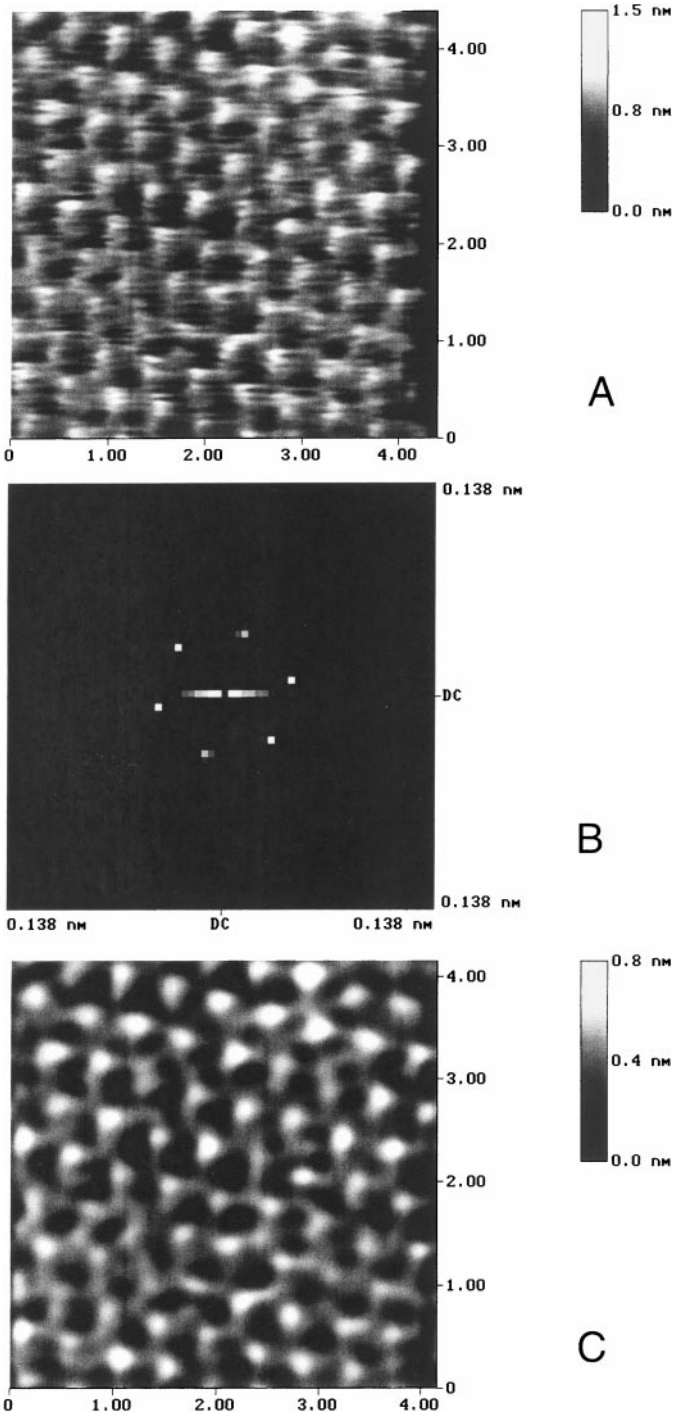

FIG. 3. Contact mode AFM images of the (001) plane of the steamed pillared rectorite before MAT evaluation: (A) raw image; (B) 2DFFT spectrum; (C) filtered image after application of a 2DFFT routine with the FFT attenuation band cutoff set to 8.

where the location of the spots in the fast Fourier transform (FFT) represents the mean distance between rows of spots in the real image. The images in Figs. 2 and 3 possessed FFTs where the spots on the hexagon did not vary more than 20% from each other. Only images consistent with the lattice parameters of the siloxane layer were considered. Images that did not conform to this criterion were disregarded to minimize the possible impact of thermal drift. The cross-section analysis on these images was always along, or nearly along, the fast-scan direction to further reduce the effects of drift. The distance between a series of bright spots was then measured and the mean distance calculated and used to obtain the mean and standard deviation for d_c shown in Table 1; d_c is the next-neighbor distance between white spots. The mean and standard deviation for d_l were measured in the same manner; d_l is the lateral distance between white spots. The cross sections were again taken along the fast-scan direction. The reported d_l (and d_c) is a mean of the means measured from the aforementioned images; these distances are shown in Fig. 2C.

RESULTS AND DISCUSSION

When an AFM is operated in a contact mode, the tip of the cantilever is in constant contact with the surface where it fluctuates according to the surface topography in a manner controlled by repulsive forces. This mode of operation provides high resolution but it can also provide artifacts resulting from morphologic deformation induced by the shape of the probe and by the rigidity of the cantilever in use. Furthermore, as sample softness increases, resolution decreases, indicating that the elasticity of the surface affects image formation in soft samples (13). The imaging force, the large contact area between the tip and the surface, the tip profile, and the viscoelastic properties of the samples are the main source of image artifacts while studying hard surfaces. Contact mode image artifacts resulting from tip–surface interactions can be minimized by operating the AFM in a tapping mode but at the expense of resolution. However, examples of atomic-scale resolution have been obtained while operating AFMs in either contact (12, 14) or noncontact (15) mode. By rotating the image, changing scan speeds and time, changing imaging forces, and acquiring images invariant with time, artifacts can be identified (16) and separated from real features when studying the coked surface of a pillared rectorite catalyst with an AFM operating in contact mode.

Figure 1B shows an ideal representation of the basal surface of the rectorite tetrahedral sheet. The tetrahedral sheet consists of a well-ordered honeycomb structure characterized by hexagonal arrangement of oxygens (O–O distance of 0.28 nm) forming hexagonal holes 0.26 nm in diameter. The apical oxygen of the SiO_4 points into the plane and therefore cannot be seen in Fig. 1B. The surface structure in Fig. 1B is in good agreement with the nanometer-scale details shown in Fig. 2 for the surface of the calcined pillared rectorite catalyst under study. The image in Fig. 2 consists of a collection of white spots in hexagonal arrangements

having nearest-neighbor distance $d_c = 0.54$ nm and lateral distance $d_l = 0.97$ nm in agreement with the repeat distances (0.54×0.96 nm) of the rectorite silicate layer (see Table 1). Although it is uncertain that the individual white spots in these images represent individual atoms or molecules, the periodicities in the image can reasonably be expected to reflect the distances between unit cells in the clay silicate layer. Similar images have been obtained for the surfaces of other smectite samples (9–11).

When imaging in air, the clay surface could be covered with a monolayer of water. However, the AFM cantilever can act as a molecular broom, thus removing weakly sorbed impurities from the surface (13, 14). Large quaternary ammonium cations (17) as well as trimeric Co clusters (18) have been rearranged, but not removed, from the surface of microporous materials during imaging. All images of the clay (001) surface obtained in this study resemble that in Fig. 2. The preservation of the repeat distances of the siloxane surface in these images indicates that, under the synthesis conditions used (19), the surface of the pillared rectorite catalyst is essentially free from Al species.

Steaming of the pillared clay catalyst causes minor deformations of the honeycomb structure without affecting the clay surface topography (Fig. 3). After gas oil cracking under MAT conditions the calcined and steamed clay particle assumes a deep black coloration owing to a 10.2 wt% carbon deposition (4). Carbon generation in clays is two to three times higher than in HY-type zeolites (5). Micrometer-scale (2.5×2.5 μm) AFM images in Figs. 4A and 4B do not reveal major variation in surface morphology. Moreover, properties such as surface roughness are expected to be affected by coke deposition. However after comparing seven 5×5-μm images of steamed and coked pillared rectorites, the average value of the mean roughness (20) increased only from 147 to 157 nm; the standard deviations were 35 and 36, respectively. This slight increase in surface roughness indicates that coke, after pore filling the pillared clay microspace, forms a fairly homogeneous film of carbonaceous deposits on the outer surface, thus imparting to the catalyst its deep black coloration. In fact, the contact mode micrometer-scale AFM image in Fig. 4 shows that the surface of the coked pillared rectorite sample is fairly flat and that it does not contain recognizable separate and distinct agglomerates of carbonaceous deposits as reported for other types of catalysts (8). These results lend support to reports that coke formation and the mode of coke deposition depend on the nature of the surface and on the type and location of its active sites (8).

Figure 5 shows a molecular-scale AFM image of the coked surface. The raw data have been filtered with a 2DFFT routine to generate a new image in which random noise has been removed (see Fig. 5C). By comparing the raw data in Fig. 5B with the filtered data in Fig. 5C, it can be seen

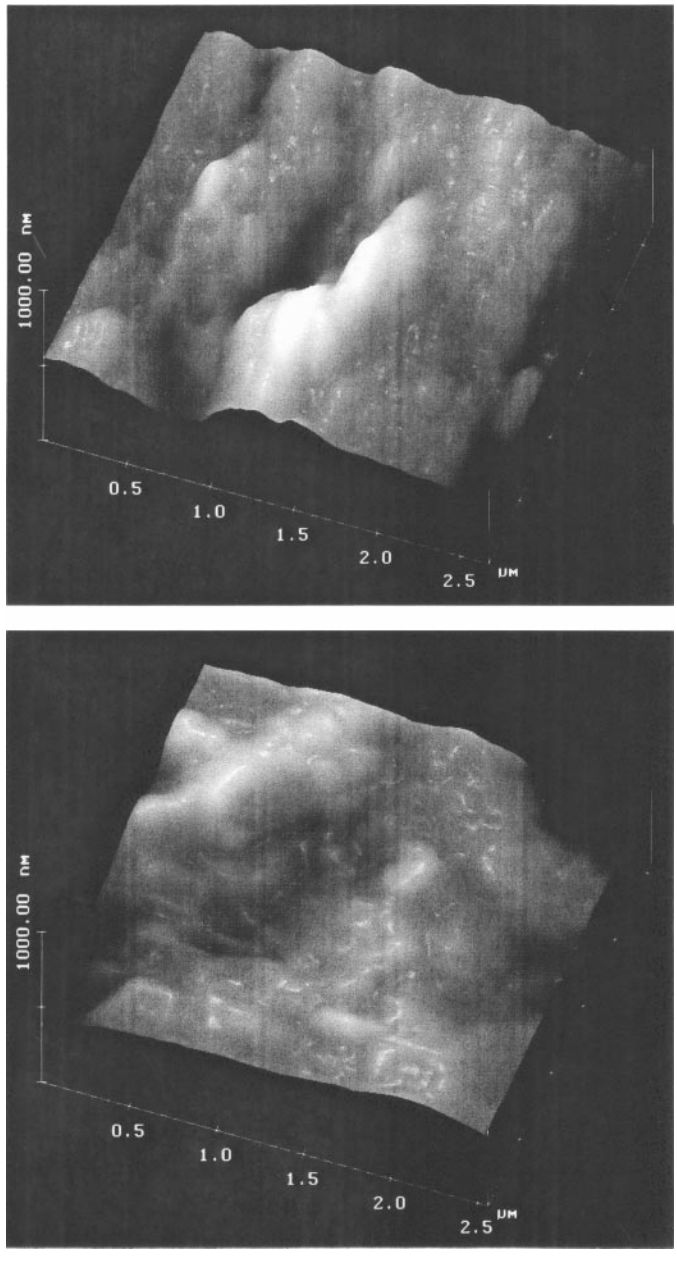

FIG. 4. Contact mode, micrometer-scale image of the pillared rectorite surface after steaming (top) and MAT evaluation (bottom). The spent catalyst contains 10.2 wt% coke.

that artifacts have not been introduced into the image by the filtering routine used. The nanometer-scale image of the layer of coke that covers the clay surface surprisingly shows a collection of spots, irregular in size and shape, arranged in a distorted but easily recognizable hexagonal arrangement (see Fig. 5). Repeat distances ($d_c = 0.70$ nm and $d_l = 1.23$ nm) in the image are larger then those measured for the steam-aged pillared rectorite before MAT evaluation (see Table 1).

Images in Figs. 5 are geometrically similar to calculated images for graphite (21). However, the much shorter (0.245 nm) next-neighbor distance between carbon atoms in graphite allows for easy differen tiation between the two types of surfaces. Thus it appears that during gas oil cracking under MAT conditions, coke is deposited inside as well as outside the pillared rectorite microspace. High-molecular-weight hydrocarbons too large to diffuse into the clay catalyst micropores are preferentially deposited and decomposed near the basal oxygens of SiO_4 units that form the clay silicate layer (see Fig. 6). After the oxidative regeneration in air (at 760°C/2 h) the layer of coke is removed and the regenerated pillared rectorite catalyst resumes its light pink coloration and the molecular-scale dimensions of the clay silicate layer reappear (see Table 1 and Fig. 7).

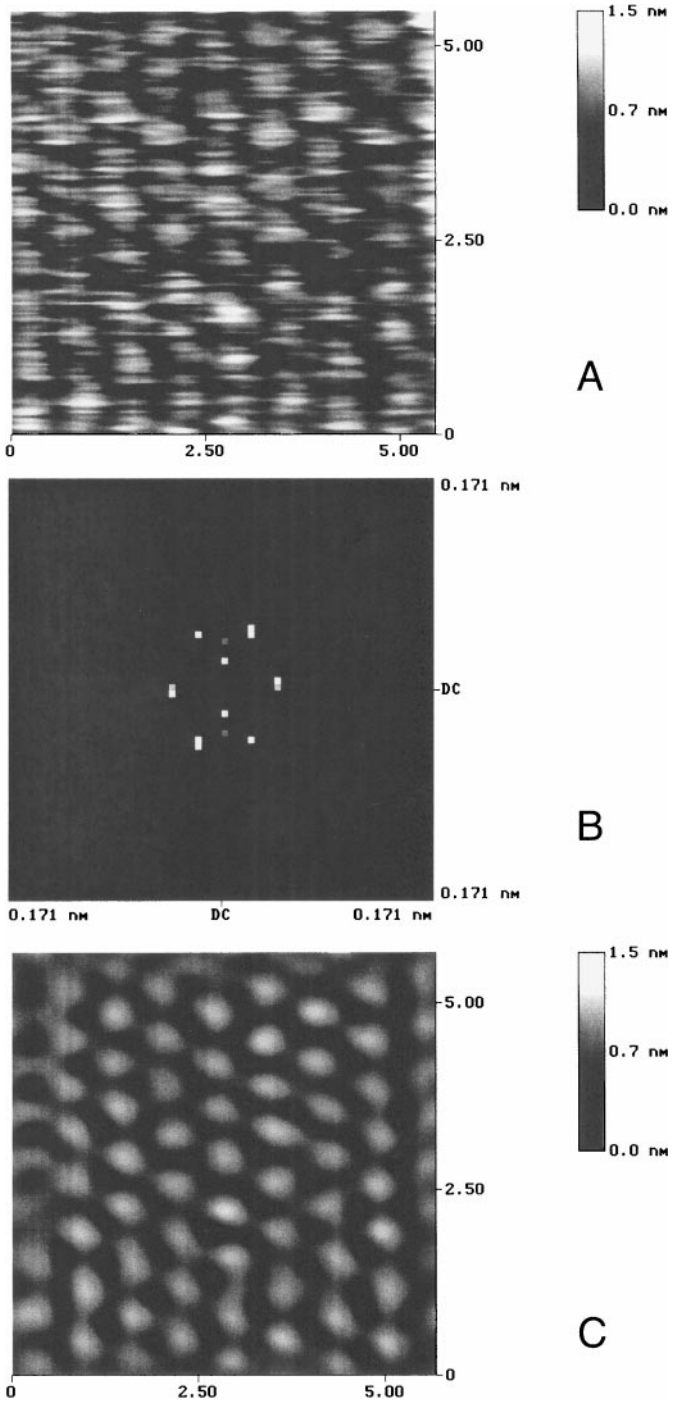

FIG. 5. Contact mode AFM images of the (001) plane of the pillared rectorite after steaming and MAT evaluation. The spent catalyst contains 10.2 wt% coke. (A) Raw image. (B) 2DFFT spectrum. (C) Nanometer-scale details of the image in (A) after application of a 2DFFT routine with the FFT attenuation band cutoff set to 8.

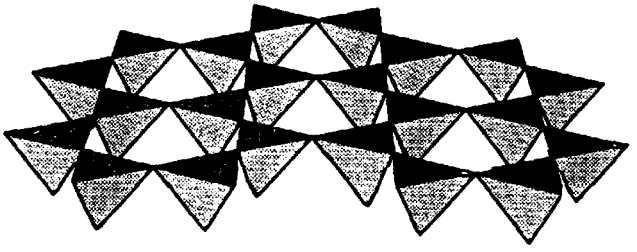

FIG. 6. Schematic representation of the rectorite (001) plane indicating the preferred regions of coke deposition (dark areas) on the tetrahedral sheet.

SUMMARY AND CONCLUSIONS

Deactivation of pillared rectorite catalysts while cracking gas oil under MAT conditions occurs because of high coke formation (4). During the cracking reaction, the sorption, formation, and retention of hydrocarbons inside the pillared rectorite microstructure is believed responsible for most of the high (10.2%) coke formation and rapid catalyst deactivation.

Gas oil components too large to penetrate the pillared rectorite micropores are segregated on the outer surface where they decompose, forming a layer of coke (with ordered structure but with lattice spacings other than graphite) that gives to the spent catalyst its black coloration; the nature of the coke layer is not known. High-molecular-weight compounds in gas oil contain heteroatoms such as N, S, Ni, and V that could react with the silicate layer (22). The preferential deposition of carbonaceous residues near the three basal oxygens of SiO_4 units represented in Fig. 6 may be the result of metal–oxygen interactions on the tetrahedral layer surface. Similar results have been reported for pillared rectorites contaminated with V-naphthenates dissolved in toluene (22); the preservation of the tetrahedral sheet nanometer-scale parameters was attributed to the formation of $-Si(O)_3V{=}O$ groups (22). Evidence of graphite formation or of coke deposition in the surface hexagonal holes was not observed in any of the samples examined.

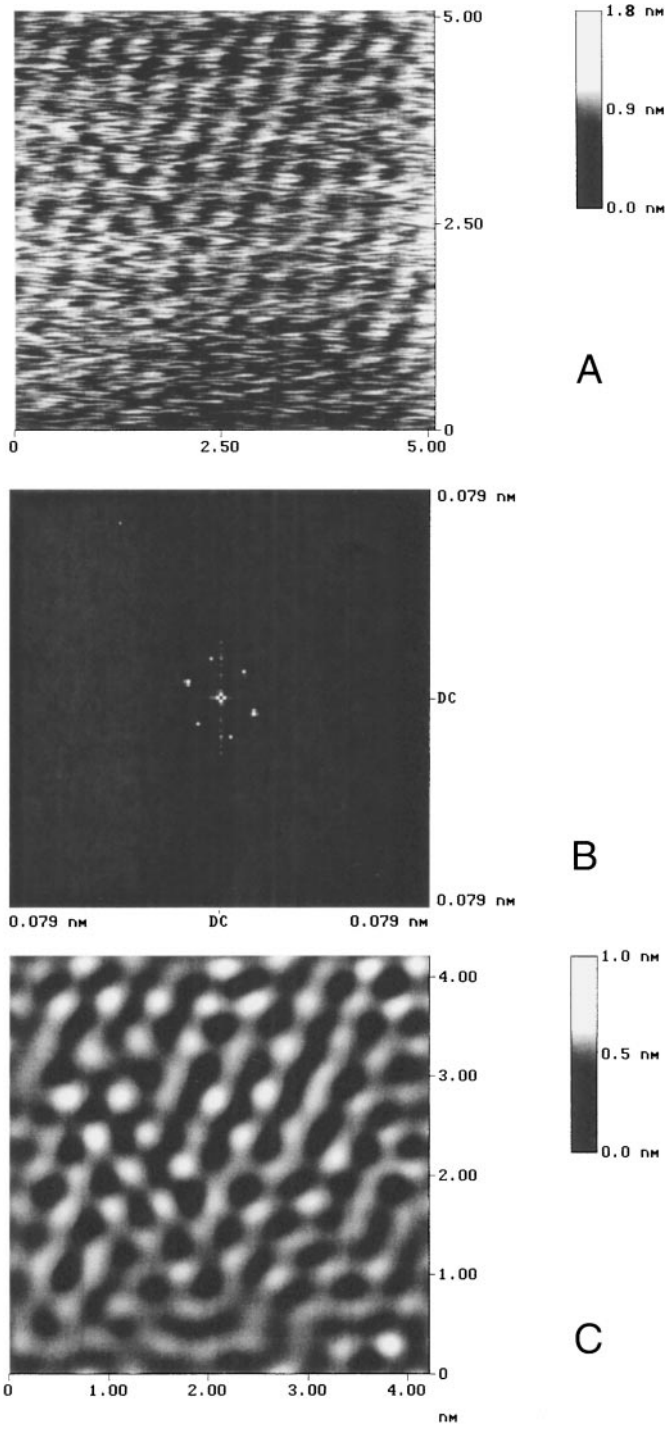

FIG. 7. Contact mode AFM images of the (001) plane of the regenerated rectorite after the removal of coke deposits at 760°C/2 h in air: (A) raw image; (B) 2DFFT spectrum; (C) filtered image after application of a 2DFFT routine with the FFT attenuation band cutoff set to 8.

Neither steaming nor the oxidative decomposition of coke deposits degrades the clay catalyst surface structure and after coke removal the molecular parameters of the siloxane surface are restored. The retention of surface structure after thermal and hydrothermal treatments required for MAT and catalyst regeneration, together with the retention of surface area and pore volume, explains the observed restoration of cracking activity in the regenerated pillared rectorite catalyst (4).

ACKNOWLEDGMENTS

This work was supported in part by NATO Collaborative Grant CRG-971497 to M.L.O. Thanks are also due B. Drake for valuable discussions during the initial part of this research.

REFERENCES

1. Grim, R. E., "Clay Minerology," McGraw–Hill, New York, 1968.
2. Guan, J., Min, E., Yu, Z., Zheng, H., and Liang, Y., China–Japan–USA Symposium on Hetero. Catal. Related to Energy Problems, Paper BO2C, p. 7 (1982).
3. Guan, J., Min, E., and Yu, Z., U.S. Patent 4,757,040 (1987).
4. Occelli, M. L., "Scientific Basis for the Preparation of Heterogeneous Catalysts, Fifth International Symposium" (G. Poncelet, P. A. Jacobs, P. Grange, and B. Delmond, Eds.), p. 287. Elsevier, Amsterdam, 1991.
5. Occelli, M. L., and Lester, J., *Ind. Eng. Chem. Prod. Res. Dev.* **24**, 27 (1985).
6. McIntyre, B. J., Salmeron, M., and Samorjai, G. A., *J. Catal.* **164**, 184 (1999).
7. Trimm, D. L., *in* "Progress in Catalysts Deactivation" (J. L. Figueiredo, Ed.), p. 65. Nijhoff, The Hague/Boston/London, 1982.
8. Gaigneauex, E. M., Ruiz, P., Wolf, E. E., and Delmond, B., *J. Catal.* **172**, 247 (1997).
9. Hartman, H., Sposito, G., Yang, A., Manne, S., Gould, S. A. C., and Hansma, P., *Clays Clay Miner.* **38**, 337 (1990).
10. Lindgreen, H., Garnaes, J., Hansen, P. L., Besenbacher, F., Laegsgaard, E., Steinsgaard, P., Gould, S. A. C., and Hansma, P., *Am. Miner.* **76**, 1218 (1990).
11. Occelli, M. L., Drake, B., and Gould, S. A. C., *J. Catal.* **142**, 337 (1993).
12. Wicks, F. J., Henderson, G. S., and Vrdolijak, G. A., "Atomic and Molecular Scale Imaging of Layered and Other Mineral Structures: Scanning Probe Microscopy of Clay Minerals" (K. L. Nagy and A. E. Blum, Eds.), CMS Workshop Lectures, Vol. 7, p. 92. Clay Mineral Soc., Boulder, CO, 1994.
13. Wawkuschewski, A., Cantow, H.-J., and Magonov, S. N., *Adv. Mater.* **6**, 476 (1994).
14. Ohnesorge, F., and Binnig, G., *Science* **260**, 1451 (1993).
15. Giessell, R., *Science* **267**, 68 (1995).
16. Nagy, K. L., and Blum, A. E. (Eds.), "Scanning Probe Microscopy of Clay Minerals," CMS Workshop Lectures, Vol. 7, Clay Mineral Soc., Boulder, CO, 1994.
17. Weisenhorn, J. E., MacDougal, J. E., Gould, S. A. C., Cox, D. S., Wise, W. S., Maivod, P., Elings, V. B., Hansma, P. K., and Stucky, G. D., *Science* **247**, 1330 (1990).
18. Thomas, S., Bertrand, J. A., Occelli, M. L., Stencel, J. M., and Gould, S. A. C., *Chem. Mater.* (1999).
19. Thomas, S., and Occelli, M. L., *Clays Clay Miner.* (2000).
20. "Nanoscope Command Reference Manual," Digital Instrument," pp. 12, 74, Santa Barbara, CA, 1997.
21. Gould, S. A. C., Burke, K., and Hansma, P. K., *Phys. Rev. B* **40**, 5363 (1989).
22. Occelli, M. L., Gould, S. A. C., and Drake, B., *J. Mol. Catal.* **100**, 161 (1995).